ORIGINAL ARTICLE

Design and Evaluation of a Multi-degree-of-freedom Piezoelectric Microactuator and its Applications

Sheng-Chih Shen[1, 2, 3,*] and Yi-Chen Chen[1, 2, 3, 4]

[1]*Department of Systems and Naval Mechatronic Engineering, National Cheng Kung University, Taiwan*
[2]*Research Center for Energy Technology and Strategy, National Cheng Kung University, Taiwan*
[3]*Center for Micro/Nano Science and Technology, National Cheng Kung University, Taiwan*
[4]*Industrial Technology Research Institute (ITRI), Taiwan*

(**Received** 18 June 2013; **Accepted** 7 July 2013; **Published on line** 1 December 2013)

*Corresponding author: scshen@mail.ncku.edu.tw

DOI: 10.5875/ausmt.v3i4.208

Abstract: A novel multi-degree-of-freedom (MDOF) microactuator was developed using a symmetric piezoelectric plate and a Ni–Co alloy micro-pusher element. A LIGA-like technique was employed to manufacture a Ni–Co alloy micro-pusher, which was then attached at the midpoint of the long side of a piezoelectric plate with dual electrodes to construct a symmetric piezoelectric pusher element (SPPE). The proposed approach integratese the concept of bricks and three different SPPE vibration modes were designed to develop a MDOF motion platform able to rotate a spherical device along three perpendicular axes. This MDOF microactuator consisted of a stator and a rotor. The stator was created from two mutually orthogonal sets of parallel SPPEs to form a MDOF motion platform, and the rotor was a spherical device. Experiments demonstrated the MDOF microactuator with working frequencies along the X, Y, and Z axes of 223.4 kHz, 223.2 kHz, and 225 kHz, respectively, and the respective rotation speeds reached 50 rpm, 52 rpm, and 180 rpm. This MODF microactuator may be used in a number of applications, such as sun-tracking systems for green energy harvesters and devices which can – eyeball-like - simultaneously and autonomously rotate along three axes for use in the biomedical field.

Keywords: MEMS; piezoelectric actuator; sun-tracking system; multi-degrees-of-freedom motion

Introduction

Recent advances have been made in the accuracy of micromechanical devices and micro-optic devices, raising the need for small and high-precision actuators. In addition, robots are being miniaturized to produce human-like motion, and such robots require microactuators that can generate dexterous, precise motions, such as multi-degree-of-freedom (MDOF) microactuators. Electromagnetic and piezoelectric actuators are currently widely available. Electromagnetic actuators are constructed using components such as magnetic materials, coils, gears, and screws, and induce a magnetic force to move the rotor, achieving multi-degree motion; however, the magnetic field strength is limited by the size of the microactuator, and reducing the size of the components results in a corresponding reduction in energy output. Magnetic actuators are inefficient in the power range below 30W [1]. Therefore, an electromagnetic actuator is unfavorable for miniaturization for use as a high-power microactuator. Piezoelectric actuators are designed using a different vibration mode and can easily achieve multi-degree motion, and hence these actuators have a relatively simple structure and are much smaller in terms of volume and weight than electromagnetic actuators. In other words, the piezoelectric actuator employs a frictional force to drive the spherical rotor. According to the scaling law, as the scale decreases, the electromagnetic force decreases more rapidly than the friction force [2]. Therefore, piezoelectric actuators are suitable for applications requiring miniaturization.

Current multi-DOF piezoelectric microactuators can be classified into two groups based on their driving methods: ring-shaped vibrators with traveling waves, and

pusher-shaped vibrators with standing waves. Ring-shaped vibrators generally have a disk-like structure, whereas pusher-shape vibrators are rectangular and have a pusher. In the early 1990s, Toyama et al. developed a ring-shaped multi-DOF piezoelectric actuator based on the driving principle of a traveling wave [3], which was the forerunner of the current multi-degree piezoelectric actuators. In 2001, Takemura et al. [4, 5] designed a multi-DOF micro-actuator with a cylindrical configuration that could generate three vibration modes: two bending and one longitudinal. Applying a different driving frequency to the electrodes on a piezoelectric plate generates a dual-phase mode to drive the ball rotor, achieving multi-degree motion. These studies achieved rotor rotation along each axis by employing microactuators that use a ring-shaped vibrator and a dual-phase mode to drive the ball.

Takemura et al. [6] developed a multi-DOF piezoelectric microactuator with a compact plate stator and a spherical rotor that used pusher-shaped vibrators with a dual-phase mode. Otokawa [7] proposed a multi-DOF piezoelectric microactuator consisting of four pusher-shaped vibrators with a single-phase mode. Single-phase mode multi-DOF microactuators with pusher-shaped vibrators commonly use a resonant frequency to create independent vibration modes in each piezoelectric plate, thus allowing the rotor to rotate on three perpendicular axes. Therefore, multi-DOF microactuators driven by a single phase are simpler and easier to downsize than dual-phase microactuators [8]. A single-phase mode actuator was developed by switching different single-phase modes for each vibrator to promote rotor movement [9], whereas dual-phase mode actuators must be simultaneously excited by the longitudinal vibration mode and the bending vibration mode to create a motion trajectory [10, 11]. The driver circuit of the dual-phase mode actuators requires at least two groups of driving signals to achieve synchronization resonance, but it is difficult to precisely control the two frequencies that must be in complete mutual correspondence.

This study proposes a novel multi-DOF piezo-electric microactuator with pusher-shaped vibrators, which only requires the combination of three vibrators driven by a single phase to move a hemisphere concentrator lens along three perpendicular axes. The proposed system is then applied to a pocket sun-tracking system and a high-power eyeball-like microactuator.

Sheng-Chih Shen received the BS and MS degrees in automatic control engineering from Feng Chia University, Taichung, Taiwan, in 1996 and 1998, respectively, and the Ph.D. degree in engineering from the Engineering and System Science Department, National Tsing Hua University, Hsinchu, Taiwan, in 2002. He was a researcher in the MEMS Division, Industrial Technology Research Institute, Tainan, Taiwan, from 2002 to 2007, and a visiting scholar in the field of MEMS at Carnegie Mellon University, Pittsburgh, PA, from 2004 to 2005. He has been with the Department of Systems and Naval Mechatronic Engineering, National Cheng Kung University, Tainan, as an associate professor since 2010. His current research interests focus on MEMS, microactuator, and LIGA process.

Yi-Chen Chen is the Ph.D student in Department of Systems and Naval Mechatronic Engineering, National Cheng Kung University.

DESIGN AND FABRICATION

Structure of the SPPE Element

A driving voltage was applied on a square piezoelectric plate with a piezoelectric strain constant of d_{31}, generating an extension/contraction movement at the edges of the plate. A symmetric piezoelectric pusher element (SPPE) was then designed using two square piezoelectric plates to form a rectangular piezoelectric plate based on this extension/contraction movement. For the SPPE element, SPPE polarization occurred along the thickness dimension (Z direction), which generated the d_{31} piezoelectric strain constant (Figure 1). Two symmetric square electrodes A and B were then placed on the front side of the large surface (X–Y plane). Each electrode covered one-half of the surface, whereas the rear surface had a single electrode that served as a common drain. The micro-pusher was attached at the midpoint P of one long edge of the piezoelectric plate. Movement of the midpoint P in different directions was achieved by switching the applied voltage between the symmetric electrodes.

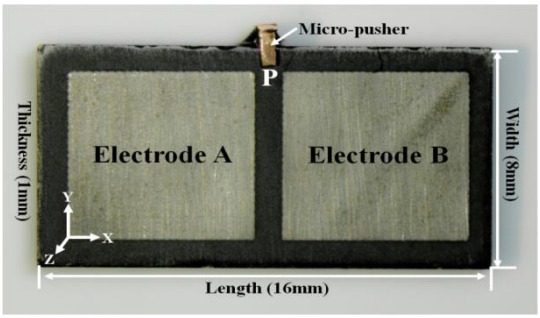

Figure 1. Structure of a symmetric piezoelectric pusher element (SPPE).

Figure 2 shows the fabrication process for the micro-pusher using an LIGA-like technique. This micro-electroforming technique was used to electrodeposit metals onto a structure defined by photoresist masks. The micro-pusher was formed after removing the photoresist masks. Figure 2 shows the sputtering of the Au seed layer, the photolithograph process using photoresist SU-8, and the Ni–Co electroformation to fabricate the micro-pusher. An electroforming layer of low stress and high hardness was required; thus, 0.5% of stress-reducing agents were added, and the current density was controlled to reduce

the internal stress to zero. The electrolyte compositions and operating instructions were as those used by Shen et al. [12]. The substrate was then immersed in a stripper to remove the micro-pusher, and a Ni–Co alloy with a Vickers hardness value (HV) of approximately 550 was applied to develop the SPPE. The length, width, and thickness of the micro-pusher were 1.5 mm, 3 mm, and 0.5 mm, respectively. The micro-pusher was mounted at midpoint P of the SPPE X–Z plane to enhance its driving capability. This novel SPPE structure completely avoids the abrasion problem of ceramic micro-pushers by adopting a Ni–Co alloy micro-pusher.

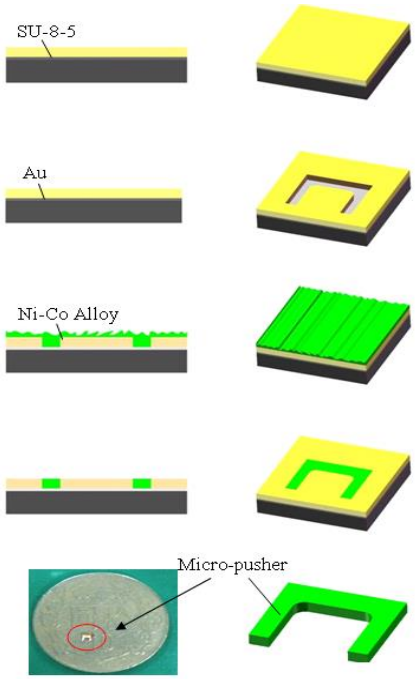

Figure2. Micro-pusher fabrication process using an LIGA-like technique.

Dynamic Analysis of the SPPE

The SPPE is excited by generating a signal on one of the electrodes on the front side. This excitation signal is the resonant frequency of a vibration mode of the SPPE. This mode is that of a two-dimensional standing wave, and can be viewed as the superposition of standing waves in two directions. Applying a driving voltage on the SPPE can generate micro-pusher movement in different directions. Therefore, the displacement of the micro-pusher (i.e., midpoint P) can be expressed as

$$\left(\frac{u_x}{-2A_x\cos\lambda y\cos\xi x\sin\frac{\varphi}{2}}\right)^2+\left(\frac{u_y}{2A_y\sin\lambda y\cos\xi x\cos\frac{\varphi}{2}}\right)^2=1. \quad (1)$$

where u is the displacement, A is the amplitude, and λ and ξ are the wave numbers. The micro-pusher displacement can be expressed as in (1) because the SPPE has a standing-wave driving component.

Equation (1) shows that when φ=0 or ϕ=π, the micro-pusher has a straight-line trajectory along the Y direction or X direction, and when $\varphi\neq0$ or $\varphi\neq\pi$, the micro-pusher has an elliptical trajectory. Consequently, the micro-pusher amplitude along a line is inclined with respect to the plate surface. Based on Eq. (1) , the three vibration modes of the SPPE can be obtained when both electrodes A and B are simultaneously excited with the signal-phase mode. This is defined as mode (1, 1) and φ=0. This indicates that the micro-pusher has no displacement in the X direction and a straight-line trajectory in the Y direction. When only electrode A is excited, this is defined as mode (1,0). In this case, the micro-pusher moves in the direction of the inclination at Quadrant I. When only electrode B is excited, this is defined as mode (0,1). In this case, the micro-pusher moves in the direction of the inclination at Quadrant II.

The driving principle of the multi-DOF piezoelectric actuator is based on the movement of midpoint P, which is generated by the vibration of the SPPE. Therefore, this study used ANSYS software to investigate the behavior of the SPPE and to design the multi-DOF piezoelectric actuator. In the simulation, the PZT material properties of d_{31}, electromechanical coupling coefficient, quality factor, and density were 171 pm/V, 0.34, 1800, and 7.75 g/cm^3, respectively. The fixed points of the SPPE were designed on the oscillation nodes to prevent the vibration mode from reducing the driving efficiency of the multi-DOF piezoelectric actuator. The simulation results demonstrate that the fixed nodes could be located in two zones on the long side of the SPPE, at 3.5–4.5 mm and 11.5–12.5 mm.

A driving voltage was applied to electrodes A and B to verify the trajectory of the micro-pusher. By generating different vibration modes, the SPPE produced three different trajectory directions on the micro-pusher. Table 1 shows the dynamic SPPE behavior of the micro-pusher under a certain driving voltage and different vibration mode. Table 1(A) shows the vibration mode (1,1), in which both electrodes A and B are excited. Table 1(A)(II) shows that when the driving voltage is in the peak position ($V=V_{max}$), the micro-pusher of the SPPE exhibits an extension movement in which the micro-pusher moves in a straight line and achieves maximum displacement in the Y direction. Table 1(A)(IV) shows that when the driving voltage is in the trough position ($V=-V_{max}$), the micro-pusher of the SPPE exhibits a contracting movement. In Table 1(A)(I) and 1(A)(III), when the driving voltage is at position (V = 0), the

micro-pusher of the SPPE is stable The motion points can be obtained from the excitation electrode toward the floating electrode (Tables 1(B) and 1(C)). Therefore, this study employs two parallel SPPEs to design and fabricate the multi-DOF piezoelectric actuator.

Design of the MDOF microactuator

The structure of the MDOF microactuator is shown in Figure 3(a), and includes a spherical device, four pairs of SPPEs, conductive springs, and a prototype of the MDOF eyeball-like microactuator as shown in Figure 3(b). To construct the MDOF motion platform, the micro-pushers were placed at the midpoint P of each SPPE by surface mount technology, and the four pairs of SPPEs were arranged on each side of a square grid on the substrate, mimicking LEGO® bricks. The micro-pushers were fabricated from Ni–Co alloy, which allows the vibration energy generated by the SPPE to be efficiently transmitted to the micro-pushers, thus enhancing drive efficiency.

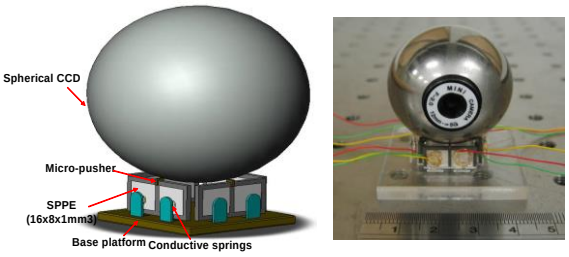

(a) (b)

Figure 3. (a) Schematic of the MDOF microactuator and (b) Prototype of the MDOF microactuator.

The driving principle of the MDOF microactuator is mainly the conversion of vibration energy by the micro-pusher into thrust force, which causes the spherical device to rotate. Three types of vibration modes in combination with different arrangements of SPPEs were used to generate thrust force, making the rotor rotate along the X-, Y-, and Z-axes. Figure 4 demonstrates how the MDOF motion platform enables the spherical rotor to rotate along the X-, Y-, and Z-axes. Figure 4(a) shows that, to drive the spherical rotor to rotate clockwise along the X-axis, a negative voltage signal ($V=-V_i$) needs to be applied on electrodes A and B of SPPE (I) with vibration mode (1,1) to cause its micro-pusher to move in the (-)Z-direction by contraction; at the same time, a positive voltage signal ($V=V_i$) must be applied on electrodes A and B of SPPE (J) with vibration mode (1,1) to cause its micro-pusher to move in the (+)Z-direction by extension; a positive voltage signal ($V=V_i$) must be applied on electrode A of SPPE (K) with vibration mode (1,0) to cause its micro-pusher to move in the (+)Y- and Z-directions by extension; and finally a positive voltage signal ($V=V_i$) needs to be applied on electrode B of SPPE (L) with vibration mode (0,1) to cause its micro-pusher to move in the (+)Y- and Z-directions by extension. Therefore, combining the four individual movements generated by each SPPE, the spherical rotor can be driven to rotate in the direction of the X-axis.

Figure 4(b) shows that, to drive the spherical rotor to move clockwise along the Y-axis, a positive voltage signal ($V=V_i$) needs to be applied on electrode B of SPPE (I) with vibration mode (0,1) to cause its micro-pusher to move in the (-)X- and (+)Z-directions by extension; at the same time, a positive voltage signal ($V=V_i$) must be applied on electrode A of SPPE (J) with vibration mode (1,0) to cause its micro-pusher to move in the (-)X- and (+)Z-directions by extension; a negative voltage signal ($V=-V_i$) also needs to be applied on electrodes A and B of SPPE (K) with vibration mode (1,1) to cause its micro-pusher to move in the (-)Z-direction by contraction; and a positive voltage signal ($V=V_i$) must be applied on electrodes A and B of SPPE (L) with vibration mode (1,1) to cause its micro-pusher to move in the (+)Z-direction by extension. This combination of the four individual movements generated by each SPPE causes the spherical rotor to move clockwise along the Y-axis.

Table1. The dynamic SPPE behavior of the micro-pusher under a certain driving voltage and different vibration modes.

Vibration mode	Excitation signal	Behavior of the SPPE motion
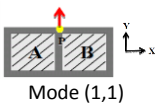 Mode (1,1)	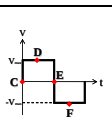	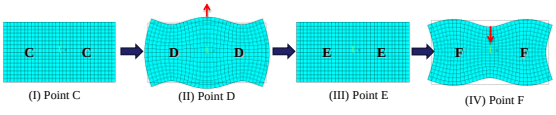 (I) Point C (II) Point D (III) Point E (IV) Point F
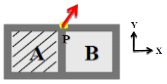 Mode (1,0)	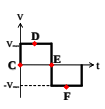	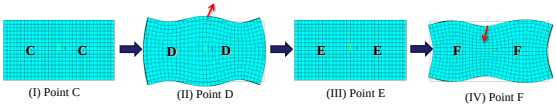 (I) Point C (II) Point D (III) Point E (IV) Point F
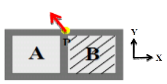 Mode (0,1)	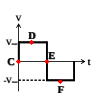	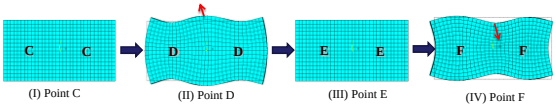 (I) Point C (II) Point D (III) Point E (IV) Point F

Finally, Figure 4(c) shows that, to drive the spherical rotor to move clockwise along the Z-axis, a positive voltage signal ($V=V_i$) needs to be applied on electrode A of SPPEs (I), (J), (K) and (L) with vibration mode (1,0) to cause the micro-pushers to move in the (+)X- and Z-directions (I), the (-)X- and (+)Z-directions (J), the (+)Y- and Z-directions (K), and the (-)X- and (+)Z-directions (L), respectively. Thus, combining the four individual movements generated by each SPPE, the spherical rotor can be driven to move clockwise along the Z-axis.

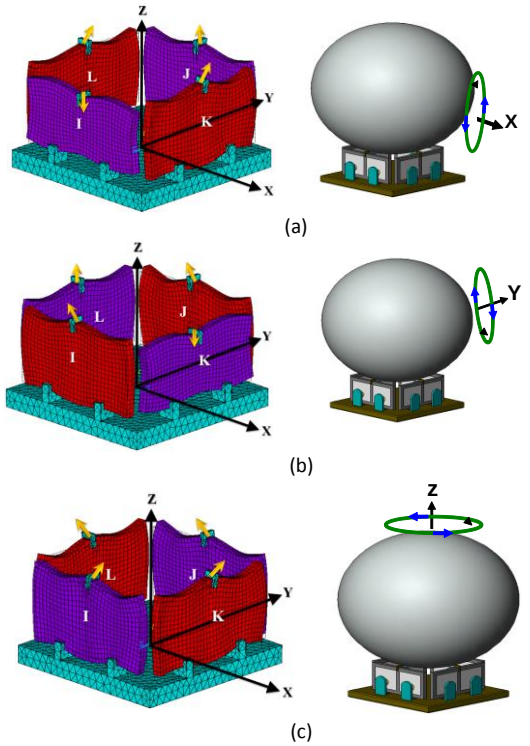

Figure 4. Clockwise rotation along (a) the X-axis; (b) the Y-axis; and (c) the Z-axis.

MEASUREMENT AND EXPERIMENT

The load characteristics of MDOF eyeball-like micro-actuators, including the relationships between rotation speed, rotor diameter, and weight, were investigated. Figure 5(a) shows the characteristics of the multi-DOF piezoelectric actuator. The driving frequency of the hemisphere concentrator lens in the X-, Y-, and Z-directions of clockwise rotation were 223.4, 223.2, and 225 kHz, with rotation speeds of 50, 52, and 180 rpm, respectively, at a driving voltage of 30Vpp. Figure 5(b) shows that, when the driving frequency reached the resonant frequency of each axis, the driving voltage was proportional to the rotation speed. When the drive voltage was 50 Vpp, the rotation speeds along the X-, Y-, and Z-axis were 90, 93, and 320 rpm, respectively. These results indicate that the rotation speeds along the X- and Y-axes are significantly lower than those along the Z-axis. Thus, rotation in the direction of the Z-axis is more efficient because the micro-pusher is better able to achieve rotation of the hemisphere concentrator lens along the Z-axis in the direction of inclination. However, for rotation of the hemisphere concentrator lens along the X- and Y-axes, the micro-pushers must be pushed in the vertical and oblique directions, and the weight of the hemisphere concentrator lens must be overcome. The difference in speed between the X and Y-axis movements is primarily due to differences in each SPPE caused by the polarization process, which in turn leads to differing degrees of thrust between the hemisphere concentrator lens and the micro-pusher.

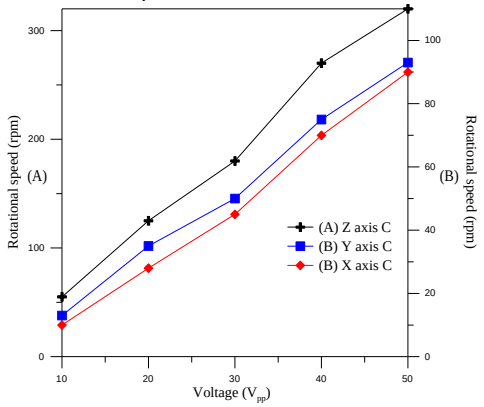

(a) Relation of driving frequency and rotation speed of multi-DOF piezoelectric actuator.

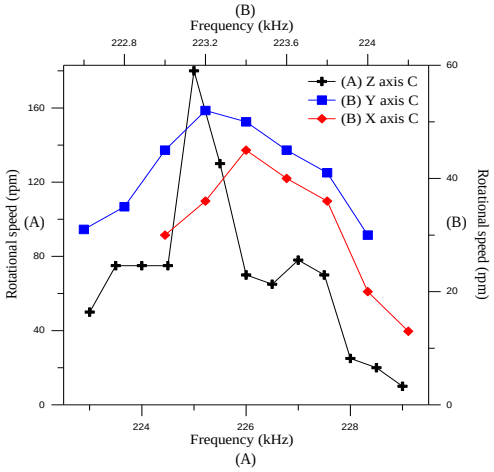

(b) Relation of driving voltage and rotation speed of multi-DOF piezoelectric actuator.

Figure 5. Characteristics of multi-DOF piezoelectric actuator.

Figure 6 shows the measured rotating accuracy of the multi-DOF piezoelectric actuator. The experiment in this study demonstrated that the 2 x 2 pocket sun-tracking system is driven by different modes and rotates around the X-, Y-, and Z-axes. Given 3 Vpp and a drive signal duty cycle of 5 ms on a multi-DOF piezoelectric actuator, the rotating accuracies of the 2 x 2 pocket sun-tracking system were 0.022°, 0.022°, and 0.007°, and the driving frequencies along the X-, Y-, and Z-axes were 223.4, 223.2, and 225 kHz, respectively. Therefore, the 2 x 2 pocket sun-tracking system can

rotate slowly with the light source (Figure 7). In addition, Figure 8 shows the high-power MDOF eyeball-like microactuator under different degrees of rotation. The MDOF motion platform was used to drive a spherical CCD and achieved multi-degree motion for precise positioning. The proposed multi-DOF piezoelectric actuator can be applied to 2 x 2 pocket sun-tracking systems for use in green energy harvesters.

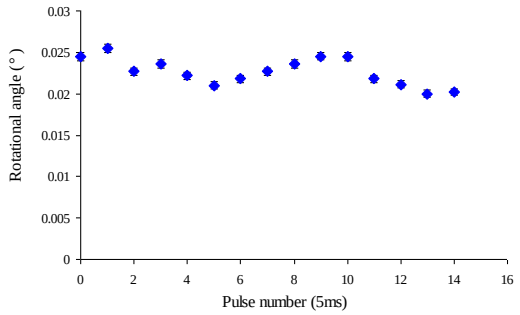

(a) X and Y rotating accuracy of the pocket sun-tracking system.

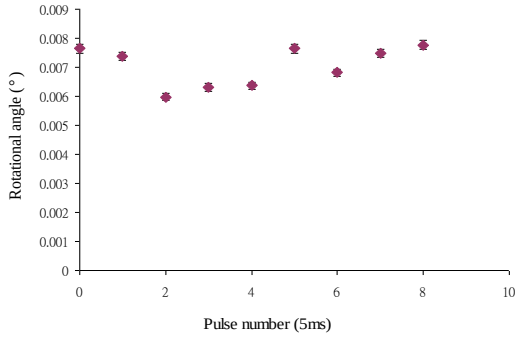

(b) Z rotating accuracy of the pocket sun-tracking system.

Figure 6. Measured rotating accuracy of the pocket sun-tracking system.

Figure 7. The 2 x 2 pocket sun-tracking system can rotate slowly with the light source.

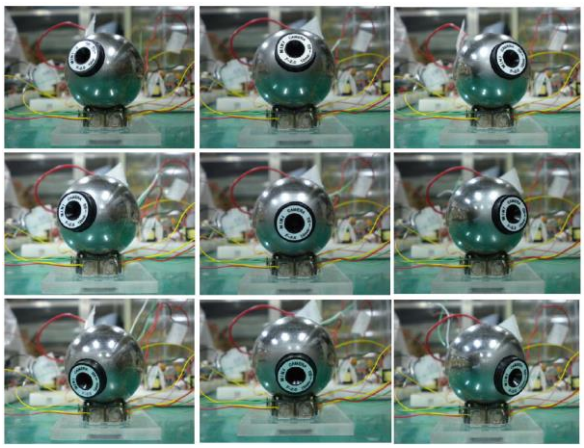

Figure 8. MDOF eyeball-like microactuator under different degrees of rotation.

Conclusion

A MDOF microactuator was developed using symmetric piezoelectric plates and Ni–Co alloy micro-pusher elements. An innovative Ni–Co alloy micro-pusher with an HV value of 550 was designed and subsequently attached at the midpoint P of the long side of a piezoelectric plate to construct an SPPE. Three different vibration modes were designed to develop a high-power MDOF microactuator based on the concept of LEGO® bricks. The characteristics of the MDOF microactuator were measured, and the driving frequencies for rotation of a spherical rotor of 350 g along the X-, Y-, and Z-axes were found to be 223.4 kHz, 223.2 kHz, and 225 kHz, respectively, while the clockwise rotation speed of the spherical rotor along the X-, Y-, and Z-axes reached 50 rpm, 52 rpm, and 180 rpm, respectively, at a driving voltage of 30Vpp. In summary, an MDOF microactuator was successfully developed. In the future, this MODF microactuator may be used for a number of applications, such as sun-tracking systems for green energy harvesters and eyeball-like devices for use in the biomedical field.

Acknowledgments

The authors would like to thank National Science Council (NSC) for providing financial support for this project (granted number: NSC 100-2628-E-006-019-MY3) and the Research Center for Energy Technology and Strategy, National Cheng Kung University.

References

[1] K. Uchino, "Piezoelectric actuators 2006 expansion from it/robotics to ecological/energy applications," *Journal of electroceram,* vol. 20, pp. 301-311, 2008. doi: 10.1007/s10832-007-9196-1

[2] S. Baglio, S. Castorina, and N. Savalli, *Scaling issues and design of mems*, Chichester: John Wiley & Sons, 2008.

[3] S. Toyama, S. Hatae, and M. Nonaka, "Development of multi-degree of freedom spherical ultrasonic motor," in *IEEE International conference of Advanced Robotics*, Pisa, Italy, 1991, vol. 1, pp. 55-60. doi: 10.1109/ICAR.1991.240476

[4] K. Takemura and T. Maeno, "Design and control of an ultrasonic motor capable of generating multi-dof motion," *IEEE/ASME Transactions on Mechatronics,* vol. 6, no. 4, pp. 499-506, 2001. doi: 10.1109/3516.974864

[5] M. Zhang, W. Guo, and L. Sun, "A multi-degree-of-freedom ultrasonic motor using in-plane deformation of planar piezoelectric elements," *Sensors and Actuators A: Physical,* vol. 148, no. 1, pp. 193-200, 2008.
doi: 10.1016/j.sna.2008.07.022

[6] K. Takemura, Y. Ohno, and T. Maeno, "Design of a plate type multi-dof ultrasonic motor and its driving characteristics," in *IEEE International Conference of Advanced Intelligent Mechatronics*, 2004, vol. 9, pp. 474-480.
doi: 10.1109/TMECH.2004.834643

[7] K. Otokawa and T. Maeno, "Development of an arrayed-type multi-degree-of-freedom ultrasonic motor based on a selection of reciprocating vibration modes," in *IEEE Ultrasonics Symposium*, 2004, vol. 2, pp. 1181-1184.
doi: 10.1109/ULTSYM.2004.1417995

[8] O. Vyshnevsky, S. Kovalev, and W. Wischnewskiy, "A novel, single-mode piezoceramic plate actuator for ultrasonic linear motors," *IEEE Transactions on Ultrasonic, Ferroelectrics and Frequency Control,* vol. 52, no. 11, pp. 2047-2053, 2005.
doi: 10.1109/TUFFC.2005.1561674

[9] K. Otokawa, K. Takemura, and T. Maeno, "A multi degree-of-freedom ultrasonic motor using single-phase-driven vibrators," *Transactions of the Japan Society of Mechanical Engineers-part C,* vol. 73, no. 2, pp. 577-582, 2007.

[10] Nanomotion LTD., "Ceramic motor," US Patent Patent 5,453,653, 1995.

[11] S. T. Ho, "Characteristics of the linear ultrasonic motor using an elliptical shape stator," *Japanese Journal of Applied Physics,* vol. 45, pp. 6011-6013,
doi: 10.1143/JJAP.45.6011

[12] C. Lu, T. Xie, T. Zhou, and Y. Chen, "Study of a new type linear ultrasonic motor with double-driving feet," *Ultrasonics,* vol. 44, Supplement, pp. e585-e589, 2006.
doi: 10.1016/j.ultras.2006.05.191

[13] S. Sheng-Chih, W. Min-Wen, and L. Chung-Jui, "Manufacture of an integrated three-dimensional structure nozzle plate using microinjection molding for a 1200-dpi inkjet printhead," *IEEE/ASME Journal Microelectro- mechanical system,* vol. 18, no. 1, pp. 52-63, 2009.
doi: 10.1109/JMEMS.2008.2009847